Supplementary Information

Proton transfer induced competing product channels of the

microsolvated $Y^-(H_2O)_n$ + CH_3I (Y = F, Cl, Br, I) reactions

Xiaoyan Ji and Jing Xie*

Key Laboratory of Cluster Science of Ministry of Education, School of Chemistry and Chemical
Engineering, Beijing Institute of Technology, Beijing 100081, China

Corresponding author:

Jing Xie jingxie@bit.edu.cn

Table of Contents

Table S1. Benchmark study of the reaction energies for PT_{CH3} pathways of $Cl^-(H_2O)_{n=0,1,2}$ + CH_3I reactions.

	Y = Cl	B97-1[a]	CCSD(T)[a,b]	Absolute Error
n = 0	$CH_2I^- + HY$	60.2(57.2)	58.8(55.8)	1.4(1.4)
n = 1	$CH_2I^- + HY + H_2O$	75.3(70.5)	73.4(68.6)	1.9(1.9)
	$CH_2I^- + HY(H_2O)$	69.1(65.5)	67.7(64.1)	1.4(1.4)
	$CH_2I^-(H_2O) + HY$	55.7(51.9)	54.3(50.5)	1.4(1.4)
n = 2	$CH_2I^- + HY + 2H_2O$	89.9(83.5)	88.6(82.2)	1.3(1.3)
	$CH_2I^- + HY(H_2O) + H_2O$	83.7(78.5)	82.9(77.7)	0.8(0.8)
	$CH_2I^- + HY(H_2O)_2$	75.3(71.7)	74.8(71.2)	0.5(0.5)
	$CH_2I^-(H_2O) + HY + H_2O$	70.3(64.9)	69.5(64.1)	0.8(0.8)
	$CH_2I^-(H_2O) + HY(H_2O)$	64.1(59.5)	63.8(59.6)	0.3(0.1)
	$CH_2I^-(H_2O)_2 + HY$	50.0(45.8)	48.0(43.8)	2.0(2.0)
	Mean absolute Error			1.2(1.2)

[a]Calculated energies in kcal/mol. Values in normal text are electronic energy without zero-point energy (ZPE) correction; enthalpy values at 298.15 K are in parentheses.
[b]The values are single point energy calculated on top of structures optimized with B97-1/ECP/d method.

Table S2. Calculated energies (kcal/mol) of the stationary points on the PES profiles of PT_{CH3} product channel for the $Y^-(H_2O)_{1,2} + CH_3I$ (Y = F, Cl, Br, I) reactions at the B97-1/ECP/d level of theory. Values without zero-point-energy (ZPE) corrections are in normal text, enthalpy values at 298.15 K are in parentheses.

Y^-	$F^-(H_2O)$	$Cl^-(H_2O)$	$Br^-(H_2O)$	$I^-(H_2O)$
$Y^-(H_2O) + CH_3I$	0.0	0.0	0.0	0.0
1HRC	-14.3 (-13.0)	-	-	-
1HTS	-13.4 (-12.7)	-	-	-
1RC	-13.5 (-12.2)	-10.4 (-9.2)	-9.6 (-8.5)	-8.1 (-7.5)
$1^{PT}TS1_a$	16.8 (16.1)	45.8 (42.4)	53.2 (49.3)	59.0 (54.7)
$1^{PT}TS1_b$	18.5 (17.7)	47.3 (43.9)	54.7 (50.8)	60.6 (56.2)
$1^{PT}TS1_c$	25.3 (24.6)	54.3 (50.8)	61.0 (57.0)	66.5 (62.2)
$1^{PT}TS1_d$	27.1 (26.6)	55.9 (52.3)	61.5 (57.5)	67.3 (62.9)
$1^{PT}TS1_e$	-	-	63.2 (59.1)	69.1 (64.6)
$1^{PT}TS2_a$	16.0 (15.1)	44.5 (40.7)	51.4 (47.1)	57.5 (52.8)
$1^{PT}TS2_b$	17.2 (16.3)	45.9 (42.4)	53.1 (49.1)	58.8 (54.4)
$1^{PT}TS2_d$	25.8 (25.1)	55.0 (51.6)	-	-
$1^{PT}TS2_e$	25.0 (24.3)	53.5 (49.8)	62.2 (58.2)	68.2 (63.8)
$1^{PT}TS2_f$	-	-	60.1 (55.8)	66.1 (55.8)
$1^{PT}PC1_a$	15.5 (15.4)	43.8 (40.8)	50.5 (47.0)	56.6 (52.5)
$1^{PT}PC1_b$	16.1 (16.0)	44.4 (41.5)	-	-
$1^{PT}PC1_c$	24.7 (24.7)	53.3 (50.2)	59.5 (56.0)	65.4 (61.3)
$1^{PT}PC1_d$	22.6 (22.7)	-	59.8 (56.2)	65.9 (61.5)
$1^{PT}PC2_a$	15.2 (14.9)	43.3 (40.1)	49.9 (46.1)	55.7 (51.4)
$1^{PT}PC2_d$	24.2 (24.1)	52.4 (49.1)	-	-
$1^{PT}PC2_e$	-	-	58.6 (54.8)	64.2 (59.7)
$CH_2I^- + HY + H_2O$	48.1 (45.7)	75.3 (70.5)	82.1 (76.9)	86.4 (80.7)
$CH_2I^- + HY(H_2O)$	38.9 (38.1)	69.1 (65.5)	76.9 (72.8)	83.0 (78.4)
$CH_2I^-(H_2O) + HY$	28.4 (27.1)	55.7 (51.9)	62.5 (58.3)	66.8 (66.2)

Y^-	$F^-(H_2O)_2$	$Cl^-(H_2O)_2$	$Br^-(H_2O)_2$	$I^-(H_2O)_2$
$Y^-(H_2O)_2 + CH_3I$	0.0	0.0	0.0	0.0
$2RC_a$	-11.3 (-9.9)	-9.4 (-8.2)	-8.8 (-7.6)	-8.8 (-7.6)
$2RC_b$	-6.4 (-5.7)	-9.2 (-7.8)	-8.6 (-7.4)	-8.6 (-7.4)
$2RC_c$	-	-8.0 (-7.1)	-7.3 (-6.4)	-7.3 (-6.4)
$2RC_d$	-	-7.1 (-6.1)	-7.0 (-5.9)	-7.0 (-5.9)
$2^{PT}TS1_a$	24.5 (23.2)	48.1 (44.2)	54.3 (49.9)	57.5 (52.8)

	$F^-(H_2O)_2$	$Cl^-(H_2O)_2$	$Br^-(H_2O)_2$	$I^-(H_2O)_2$
$2^{PT}TS1_b$	24.9 (23.6)	47.5 (43.6)	53.8 (49.4)	58.3 (53.4)
$2^{PT}TS1_c$	26.2 (24.9)	48.6 (44.7)	54.8 (50.5)	59.2 (54.4)
$2^{PT}TS1_d$	26.1 (25.5)	48.8 (44.7）	54.9 (50.4)	59.4 (54.3)
$2^{PT}TS1_e$	29.3 (28.4)	52.7 (49.0)	58.9 (54.8)	63.7 (59.0)
$2^{PT}TS1_f$	31.4 (30.5)	54.0 (50.3)	60.2 (56.0)	64.7 (60.1)
$2^{PT}TS1_g$	38.1 (37.5)	60.7 (57.2)	67.0 (63.0)	71.7 (67.3)
$2^{PT}TS1_h$	38.4 (37.4)	61.2 (57.4)	67.1 (62.8)	71.8 (67.1)
$2^{PT}TS2_a$	29.1 (27.9)	46.0 (41.7)	51.9 (47.1)	56.2 (51.1)
$2^{PT}TS2_b$	23.7 (22.3)	46.2 (41.4)	52.1 (46.8)	56.9 (51.1)
$2^{PT}TS2_c$	25.0 (23.4)	47.2 (43.1)	53.3 (48.8)	57.5 (52.6)
$2^{PT}TS2_d$	25.1 (23.4)	47.4 (43.1)	53.5 (48.8)	57.7 (52.3)
$2^{PT}TS2_e$	28.8 (28.2)	51.2 (47.3)	51.2 (47.3)	62.1 (57.2)
$2^{PT}TS2_f$	29.7 (28.6)	52.5 (48.8)	58.7 (54.4)	63.2 (58.6)
$2^{PT}TS2_g$	37.3 (36.5)	60.1 (56.7)	66.2 (62.2)	71.0 (66.5)
$2^{PT}PC1_a$	23.1 (22.4)	45.5 (42.0)	51.4 (47.3)	56.0 (51.7)
$2^{PT}PC1_b$	23.4 (22.7)	45.1 (41.9)	51.1 (47.1)	56.7 (51.2)
$2^{PT}PC1_c$	24.1 (23.5)	46.1 (42.9)	51.9 (48.2)	56.4 (52.3)
$2^{PT}PC1_d$	24.4 (23.6)	46.4 (43.0)	52.2 (48.3)	56.7 (52.4)
$2^{PT}PC1_e$	28.5 (28.2)	50.8 (47.8)	56.5 (52.7)	61.4 (57.0)
$2^{PT}PC1_f$	27.4 (27.1)	50.0 (46.8)	-	-
$2^{PT}PC1_g$	33.4 (33.4)	-	-	-
$2^{PT}PC1_h$	38.1 (37.7)	60.4 (57.1)	65.9 (61.9)	70.8 (66.2)
$2^{PT}PC2_a$	28.1 (27.6)	44.9 (41.0)	50.8 (46.2)	55.0 (50.3)
$2^{PT}PC2_b$	23.0 (21.9)	-	-	-
$2^{PT}PC2_c$	-	44.8 (41.1)	50.4 (46.2)	50.4 (46.2)
$2^{PT}PC2_d$	23.1 (21.8)	-	-	-
$2^{PT}PC2_e$	-	50.3 (46.9)	55.9 (51.9)	60.7 (56.1)
$2^{PT}PC2_g$	35.9 (35.7)	57.8 (54.6)	63.0 (59.1)	64.7 (62.8)
$2^{PT}PC2_h$	37.5 (37.1)	59.5 (56.0)	64.6 (60.5)	64.6 (60.5)
$CH_2I^- + HY + 2H_2O$	69.2 (65.1)	89.9 (83.5)	95.6 (88.7)	98.4 (91.2)
$CH_2I^- + HY(H_2O) + H_2O$	60.1 (57.7)	83.7 (78.5)	90.3 (84.6)	95.1 (88.9)
$CH_2I^- + HY(H_2O)_2$	50.5 (49.7)	75.3 (71.7)	82.1 (78.0)	87.9 (83.3)
$CH_2I^-(H_2O) + HY + H_2O$	49.6 (46.6)	70.3 (64.9)	75.9 (70.1)	78.8 (72.6)
$CH_2I^-(H_2O) + HY(H_2O)$	40.5 (39.0)	64.1 (59.5)	70.7 (66.1)	75.5 (70.3)
$CH_2I^-(H_2O)_2 + HY$	29.4 (27.5)	50.0 (45.8)	55.7 (51.1)	58.6 (53.6)

Table S3. Bond metrics for $^{PT}TS1$ transition states of the proton transfer channel for the $Y^-(H_2O)_{n=0,1,2} + CH_3I$ reactions at B97-1/ECP/d level of theory. Bond distances are in Angstrom, angles are in degree, and imaginary frequency in cm^{-1}.

					$n^{PT}TS1$			
n		C-H(Y)	C-I	H-I	H-Y	∠I-C-H(Y)	∠C-I-H(Y)	frequency
0	F^-	2.968	2.334	2.547	0.944	55.9	74.8	i124
0	Br^-	2.736	2.332	2.491	1.478	58.2	69.0	i309
0	I^-	2.710	2.330	2.522	1.650	59.5	67.8	i351
1	$F^-(H_2O)$	2.731	2.305	2.582	0.942	61.0	67.7	i157
1	$Br^-(H_2O)$	2.592	2.299	2.597	1.467	63.8	63.6	i328
1	$I^-(H_2O)$	2.600	2.295	2.661	1.637	65.5	62.8	i360
2	$F^-(H_2O)_2$	2.641	2.288	2.654	0.939	64.7	64.1	i173
2	$Br^-(H_2O)_2$	2.540	2.278	2.656	1.462	66.7	61.4	i313
2	$I^-(H_2O)_2$	2.570	2.280	2.763	1.630	68.7	60.7	i349

Table S4. Calculated energies (kcal/mol) of the stationary points on the PES profiles of HO⁻-S_N2 product channel for the Y⁻$(H_2O)_{1,2}$ + CH_3I (Y = F, Cl, Br, I) reactions at the B97-1/ECP/d level of theory. Values without zero-point-energy (ZPE) corrections are in normal text, enthalpy values at 298.15 K are in parentheses.

Y⁻	F⁻(H_2O)	Cl⁻(H_2O)	Br⁻(H_2O)	I⁻(H_2O)
Y⁻(H_2O) + CH_3I	0.0	0.0	0.0	0.0
1HRC	-14.3 (-13.0)	-	-	-
1RC	-	-10.4 (-9.2)	-9.7 (-8.5)	-8.7 (-7.5)
1invTS′	-6.6 (-7.2)	6.3 (6.6)	9.1 (9.5)	12.3 (12.9)
1PC′	-47.4 (-44.1)	-19.4 (-19.7)	-14.5 (-14.0)	-10.0 (-9.2)
1FSTS′	24.8 (24.0)	33.9 (34.0)	35.9 (35.9)	38.2 (38.2)
1XC′	-9.7 (-10.4)	-4.8 (-4.6)	-4.2 (-3.3)	-3.7 (-2.7)
1XTS$_{iso}$	-5.6 (-5.4)	-2.6 (-2.2)	-2.1 (-1.7)	-1.6 (-1.1)
1XTS′	-1.9 (-1.5)	-1.3 (-0.8)	-1.2 (-0.7)	-1.2 (-0.6)
1XC	-15.6 (-14.1)	-8.3 (-7.3)	-7.1 (-6.2)	-5.8 (-4.9)
1XTS	-2.3 (-1.8)	-1.5 (-1.0)	-1.3 (-0.9)	-1.2 (-0.7)
CH_3OH + I⁻ + HY	-17.9 (-17.3)	9.4 (7.4)	16.2 (13.8)	20.5 (17.7)

Y⁻	F⁻$(H_2O)_2$	Cl⁻$(H_2O)_2$	Br⁻$(H_2O)_2$	I⁻$(H_2O)_2$
Y⁻$(H_2O)_2$ + CH_3I	0.0	0.0	0.0	0.0
2HRC$_a$	-11.4 (-9.9)	-	-	-
2HRC$_b$	-11.3 (-9.9)	-	-	-
2RC	-	-9.0 (-7.8)	-8.6 (-7.4)	-7.9 (-6.7)
2invTS′$_a$	0.5 (0.9)	7.2 (8.2)	8.9 (10.0)	11.1 (12.2)
2invTS′$_b$	1.1 (1.1)	-	-	-
2invTS′$_c$	6.2 (4.5)	-	-	-
2PC′$_a$	-38.8 (-35.4)	-16.9 (-17.0)	-13.3 (-12.4)	-10.3 (-9.1)
2PC′$_b$	-37.3 (-34.2)	-15.9 (-15.7)	-12.2 (-11.5)	-8.7 (-7.7)
2PC′$_c$	-36.8 (-33.5)	-15.5 (-15.5)	-12.0 (-11.2)	-8.5 (-7.6)
2PC′$_d$	-36.7 (-33.5)	-14.2 (-14.4)	-10.8 (-10.0)	-7.0 (-6.2)
2PC′$_e$	-35.1 (-32.0)	-14.3 (-13.7)	-10.3 (-10.0)	-
2FSTS′$_a$	30.8 (31.0)	36.6 (36.7)	38.1 (38.1)	40.0 (39.9)
2FSTS′$_b$	32.1 (31.5)	38.5 (38.2)	39.7 (39.6)	41.1 (40.9)
2XC′$_a$	-6.6 (-6.5)	-4.5 (-3.5)	-4.2 (-3.1)	-3.7 (-2.7)
2XC′$_b$	-3.6 (-4.0)	-0.9 (-0.1)	-1.0 (-0.1)	-1.2 (-0.2)
2XTS$_{iso}$	-3.7 (-3.2)	-1.7 (-1.3)	-1.4 (-0.9)	-1.0 (-0.5)
2XTS′	-	-1.9 (-1.6)	-1.6 (-1.3)	-1.2 (-1.0)
2XC	-10.6 (-9.0)	-6.6 (-5.6)	-6.0 (-4.9)	-5.1 (-4.1)
2XTS	-1.5 (-0.8)	-1.9 (-1.3)	-2.1 (-1.4)	-2.4 (-1.8)
CH_3OH + I⁻ + HY + H_2O	3.3 (2.1)	24.0 (20.4)	29.7 (25.7)	32.5 (28.2)
$CH_3OH(H_2O)$ + I⁻ + HY	-2.2 (-1.8)	18.5 (16.6)	24.1 (21.8)	27.0 (24.3)
CH_3OH + I⁻ + HY(H_2O)	-5.8 (-5.5)	17.8 (15.5)	24.4 (21.6)	29.2 (25.9)
CH_3OH + I⁻(H_2O) + HY	-7.6 (-7.0)	13.1 (11.3)	18.8 (16.6)	21.7 (19.1)

Table S5. Bond metrics for invTS′ and FSTS′ transition states of the HO⁻-S_N2 channel for the $Y^-(H_2O)_{n=1,2}$ + CH_3I reactions at B97-1/ECP/d level of theory. Bond distances are in Angstrom, angles are in degree, and imaginary frequency in cm^{-1}.

	C-I	C-O	O-H	H-Y	O-Y	∠I-C-O	frequency
				invTS′			
$F^-(H_2O)$	2.522	2.191	1.246	1.116	2.362	177.9	i401
$Cl^-(H_2O)$	2.747	1.941	1.05	1.812	2.855	175.9	i398
$Br^-(H_2O)$	2.79	1.901	1.037	1.996	3.021	175.6	i382
$I^-(H_2O)$	2.84	1.854	1.025	2.256	3.258	175.2	i366
$F^-(H_2O)_2$	2.635	2.048	1.099	1.286	2.381	177.2	i419
$Cl^-(H_2O)_2$	2.753	1.933	1.008	2.01	2.971	176	i382
$Br^-(H_2O)_2$	2.777	1.909	1.001	2.213	3.153	175.8	i376
$I^-(H_2O)_2$	2.806	1.882	0.995	2.495	3.411	175.7	i372

	C-I	C-O	I-O	∠C-I-O	∠C-O-I	∠I-C-O	frequency
				FSTS′			
$F^-(H_2O)$	2.897	2.231	3.345	41.1	58.6	80.3	i530
$Cl^-(H_2O)$	3.035	2.227	3.317	40.7	62.8	76.4	i476
$Br^-(H_2O)$	3.048	2.223	3.307	40.7	63.4	75.9	i483
$I^-(H_2O)$	3.06	2.221	3.296	40.7	63.9	75.4	i485
$F^-(H_2O)_2$	2.98	2.226	3.336	40.8	61	78.1	i483
$Cl^-(H_2O)_2$	3.051	2.241	3.316	40.9	63.1	75.9	i464
$Br^-(H_2O)_2$	3.069	2.24	3.31	40.9	63.8	75.3	i467
$I^-(H_2O)_2$	3.082	2.242	3.304	40.9	64.2	74.9	i463

Table S6. Energy level of selected molecular orbital of $Y^-(H_2O)_{0,1,2}$ nucleophile as calculated with B97-1/ECP/d method.

n	0	1			2		
E (eV)	HOMO	HOMO	HOMO-1	HOMO-2	HOMO	HOMO-1	HOMO-2
$F^-(H_2O)_n$	**0.20**	**-1.53**	-1.56	-1.68	**-2.66**	-2.70	-2.86
$Cl^-(H_2O)_n$	**-0.73**	**-1.44**	-1.46	-1.62	**-2.06**	-2.15	-2.26
$Br^-(H_2O)_n$	**-0.80**	**-1.38**	-1.40	-1.55	**-1.90**	-1.98	-2.10
$I^-(H_2O)_n$	**-0.84**	**-1.31**	-1.33	-1.46	**-1.73**	-1.79	-1.92
$HO^-(H_2O)_n$	**1.15**	**-0.55**	-0.66	-1.66	**-1.44**	-1.57	-2.86

Table S7a. Energy decomposition analysis of inv-S$_N$2 and inv-S$_N$2' transition structures of Y$^-$(H$_2$O)$_n$ + CH$_3$I S$_N$2 reaction at B97-1/ECP/d level.

n	inv-S$_N$2					invTS-S$_N$2'				
	$\Delta E^{\ddagger}$	ΔE_{int}	ΔE_{prep}			$\Delta E^{\ddagger}$	ΔE_{int}	ΔE_{prep}		
kcal/mol			overall	Y$^-$(H$_2$O)$_n$	CH$_3$I			overall	Y$^-$(H$_2$O)$_n$	CH$_3$I
Y = F										
0	-17.8	-19.5	1.7	0.0	1.7					
1	-11.7	-24.3	12.6	0.9	11.7	-6.6	-23.5	16.9	3.5	13.4
2	-4.7	-25.7	21.0	2.0	19.0	0.5	-24.0	24.5	3.7	20.8
Y = Cl										
0	-8.7	-26.3	17.6	0.0	17.6					
1	-3.6	-26.4	22.8	0.3	22.5	6.3	-24.9	31.2	3.0	28.2
2	0.4	-27.2	27.6	3.4	24.2	7.2	-24.7	31.9	3.2	28.7
Y = Br										
0	-6.2	-27.2	21.0	0.0	21.0					
1	-1.9	-27.0	25.1	0.3	24.8	9.1	-24.9	34.0	2.9	31.1
2	2.0	-27.6	29.6	0.6	29.0	8.9	-24.7	33.6	3.3	30.3
Y = I										
0	-3.6	-27.9	24.3	0.0	24.3					
1	-0.1	-27.1	27.0	0.6	26.4	12.3	-25.0	37.3	2.7	34.6
2	2.2	-29.0	31.2	2.2	29.0	11.1	-24.5	35.6	3.3	32.3

Table S7b. Energy decomposition analysis of FSTS and FSTS' transition structures of $Y^-(H_2O)_n + CH_3I$ S_N2 reaction at B97-1/ECP/d level.

n	FSTS					FSTS'				
			ΔE_{prep}					ΔE_{prep}		
kcal/mol	$\Delta E^{\ddagger}$	ΔE_{int}	overall	$Y^-(H_2O)_n$	CH_3I	$\Delta E^{\ddagger}$	ΔE_{int}	overall	$Y^-(H_2O)_n$	CH_3I
Y = F										
0	14.4	-17.3	31.7	0.0	31.7					
1	24.2	-15.3	39.5	1.9	37.6	24.8	-18.9	43.7	2.4	41.3
2	31.1	-15.0	46.1	3.4	42.7	30.8	-17.8	48.6	2.6	46.0
Y = Cl										
0	31.4	-16.1	47.5	0.0	47.5					
1	33.3	-16.1	49.4	0.7	48.7	33.9	-17.5	51.4	2.3	49.1
2	35.6	-17.5	53.1	1.7	51.4	36.6	-17.7	54.3	4.1	50.2
Y = Br										
0	33.5	-15.8	49.3	0.0	49.3					
1	34.6	-15.6	50.2	0.5	49.7	35.9	-16.4	52.3	2.4	49.9
2	35.8	-18.2	54.0	1.7	52.3	38.1	-17.2	55.3	4.2	51.1
Y = I										
0	35.4	-15.2	50.6	0.0	50.6					
1	35.4	-15.5	50.9	0.4	50.5	38.2	-14.6	53.4	2.6	50.8
2	35.8	-18.4	54.2	1.7	52.5	40.0	-16.4	56.4	4.4	52.0

Table S8. Looseness (%L) and asymmetry index (%AS) of the inv-S_N2 and invTS-S_N2' transition structures.

n	inv-S_N2 transition structure	%CI‡	%CY‡	%L‡	%AS‡
0	$F^-\cdots HCH_2\cdots I$	5.03	81.12	86.15	76.09
1	$F^-(H_2O)\cdots CH_3\cdots I$	16.05	50.21	66.17	34.16
2	$F^-(H_2O)_2\cdots CH_3\cdots I$	21.41	41.13	62.54	19.72
0	$Cl^-\cdots CH_3\cdots I$	21.03	36.26	57.29	15.23
1	$Cl^-(H_2O)\cdots CH_3\cdots I$	24.43	31.73	56.16	7.30
2	$Cl^-(H_2O)_2\cdots CH_3\cdots I$	25.50	30.13	55.63	4.63
0	$Br^-\cdots CH_3\cdots I$	23.64	30.37	54.01	6.73
1	$Br^-(H_2O)\cdots CH_3\cdots I$	26.20	27.21	53.41	1.01
2	$Br^-(H_2O)_2\cdots CH_3\cdots I$	28.99	24.09	53.08	-4.9
0	$I^-\cdots CH_3\cdots I$	26.20	26.29	52.49	0.09
1	$I^-(H_2O)\cdots CH_3\cdots I$	27.41	24.38	51.79	-3.03
2	$I^-(H_2O)_2\cdots CH_3\cdots I$	29.18	22.80	51.98	-6.38
n	inv-S_N2' transition structure	%CI‡	%CO‡	%L‡	%AS‡
1	$HO^-(HF)\cdots CH_3\cdots I$	17.36	53.75	71.11	36.39
2	$HO^-(HF)(H_2O)\cdots CH_3\cdots I$	22.62	43.73	66.35	21.11
1	$HO^-(HCl)\cdots CH_3\cdots I$	27.83	36.21	64.04	8.38
2	$HO^-(HCl)(H_2O)\cdots CH_3\cdots I$	28.11	35.65	63.76	7.54
1	$HO^-(HBr)\cdots CH_3\cdots I$	29.83	33.40	63.23	3.57
2	$HO^-(HBr)(H_2O)\cdots CH_3\cdots I$	29.22	33.96	63.18	4.74
1	$HO^-(HI)\cdots CH_3\cdots I$	32.15	30.11	62.26	-2.04
2	$HO^-(HI)(H_2O)\cdots CH_3\cdots I$	30.57	32.07	62.64	1.5

Note: The transition structure looseness, %L‡, has been used in studying $X^- + CH_3Y$ S_N2 reaction in the gas phase and was found to correlate well with the inv-S_N2 barrier heights.[3] Here we employ a modified definition of transition structure looseness for inv-S_N2 (%L‡, eqn. 1) transition state for $Y^-(H_2O)_n + CH_3I$ reaction.

$$\%L^\ddagger = \%CI^\ddagger + \%CY^\ddagger \tag{1a}$$
$$\%CI^\ddagger = 100\times(r^\ddagger_{C-I} - r^{Reactant}_{C-I})/r^{Reactant}_{C-I} \tag{1b}$$
$$\%CY^\ddagger = 100\times(r^\ddagger_{C-Y} - r^{Product}_{C-Y})/r^{Product}_{C-Y} \tag{1c}$$

where $r^\ddagger_{C-I}$ and $r^\ddagger_{C-Y}$ are the C−I and C−Y bond lengths in inv-S_N2 transition structure, and $r^{Reactant}_{C-I}$ is the C−I bond length in reactant CH_3I, $r^{Product}_{C-Y}$ is the C−Y bond length in product CH_3Y. Calculated values are present in **Table S8**.

As for inv-S_N2' transition state, we also employed a similar definition of transition structure looseness (%L‡', eqn. 2).

$$\%L^{\ddagger'} = \%CI^{\ddagger'} + \%CO^{\ddagger'} \tag{2a}$$
$$\%CI^{\ddagger'} = 100\times(r^\ddagger_{C-I}' - r^{Reactant}_{C-I})/r^{Reactant}_{C-I} \tag{2b}$$

$$\%CO^{\ddagger\prime} = 100\times(r^{\ddagger}_{C\text{-}O}{}^{\prime} - r^{Product}{}_{C\text{-}O})/r^{Product}{}_{C\text{-}O} \qquad (2c)$$

Where $r^{\ddagger}_{C-I}{}^{\prime}$ and $r^{\ddagger}_{C-O}{}^{\prime}$ are the C−I and C−O bondlengths in inv-S_N2' transition structure, and $r^{Product}{}_{C-O}$ is the C−O bond length in product CH_3OH.

The geometrical asymmetry of inv-S_N2 (%AS‡) and inv-S_N2' (%AS‡') transition structures are defined by:

$$\%AS^{\ddagger} = \%CY^{\ddagger} - \%CI^{\ddagger} \qquad (3)$$
$$\%AS^{\ddagger\prime} = \%CO^{\ddagger\prime} - \%CI^{\ddagger\prime} \qquad (4)$$

Table S9. Bond metrics for halogen-bonded complex XC′ and nXTS′ of HO⁻-S_N2 channel for $Y^-(H_2O)_{n=1,2}$ + CH_3I reactions at B97-1/ECP/d level of theory. Bond distances are in Angstrom, angles are in degree, and imaginary frequency in cm^{-1}.

Nucleophile		n = 1				n = 2			
		$F^-(H_2O)$	$Cl^-(H_2O)$	$Br^-(H_2O)$	$I^-(H_2O)$	$F^-(H_2O)_2$	$Cl^-(H_2O)_2$	$Br^-(H_2O)_2$	$I^-(H_2O)_2$
nXC′	C-I	2.198	2.163	2.160	2.157	2.172	2.161	2.159	2.157
	C-O	4.797	5.000	5.032	5.081	4.921	5.008	5.031	5.063
	I-O	2.600	2.836	2.873	2.925	2.750	2.848	2.873	2.907
	∠C-I-O	178.5	177.4	177.5	177.7	178.0	178.1	178.2	178.3
nXTS′	C-I	2.145	2.145	2.146	2.146	-	2.150	2.150	2.151
	I-O	3.371	3.412	3.415	3.422	-	3.223	3.243	3.317
	∠C-I-O	134.1	143.0	144.9	146.9	-	156.1	156.7	155.1
	∠C-O-I	17.6	14.1	13.4	12.6	-	9.5	9.3	9.8
	∠I-C-O	28.3	22.8	21.7	20.4	-	14.4	14.1	15.2
	imaginary frequency	i80	i63	i54	i54	-	i49	i51	i116
nXTS$_{iso}$	C-I	2.163	2.155	2.154	2.153	2.156	2.152	2.151	2.151
	I-O	3.146	3.366	3.428	3.516	3.272	3.463	3.521	3.581
	I-Y	3.260	3.982	4.187	4.475	3.370	4.088	4.313	4.613
	O-Y	2.422	3.060	3.260	3.532	2.495	3.054	3.234	3.486
	∠Y-I-O	44.4	48.3	49.5	50.7	44.1	46.8	47.4	48.4
	imaginary frequency	i113	i66	i56	i48	i75	i63	i49	i41

Table S10. The ratio r^{vdw} of the I-O distance of the halogen-bond complexes XC′ and transition state XTS′ to the sum of van der Waals radii of atom I and O.

Y	n=1		n=2	
	XC′	XTS′	XC′	XTS′
F	0.74	0.96	0.79	-
Cl	0.81	0.97	0.81	0.92
Br	0.84	0.98	0.82	0.93
I	0.84	0.98	0.83	0.95
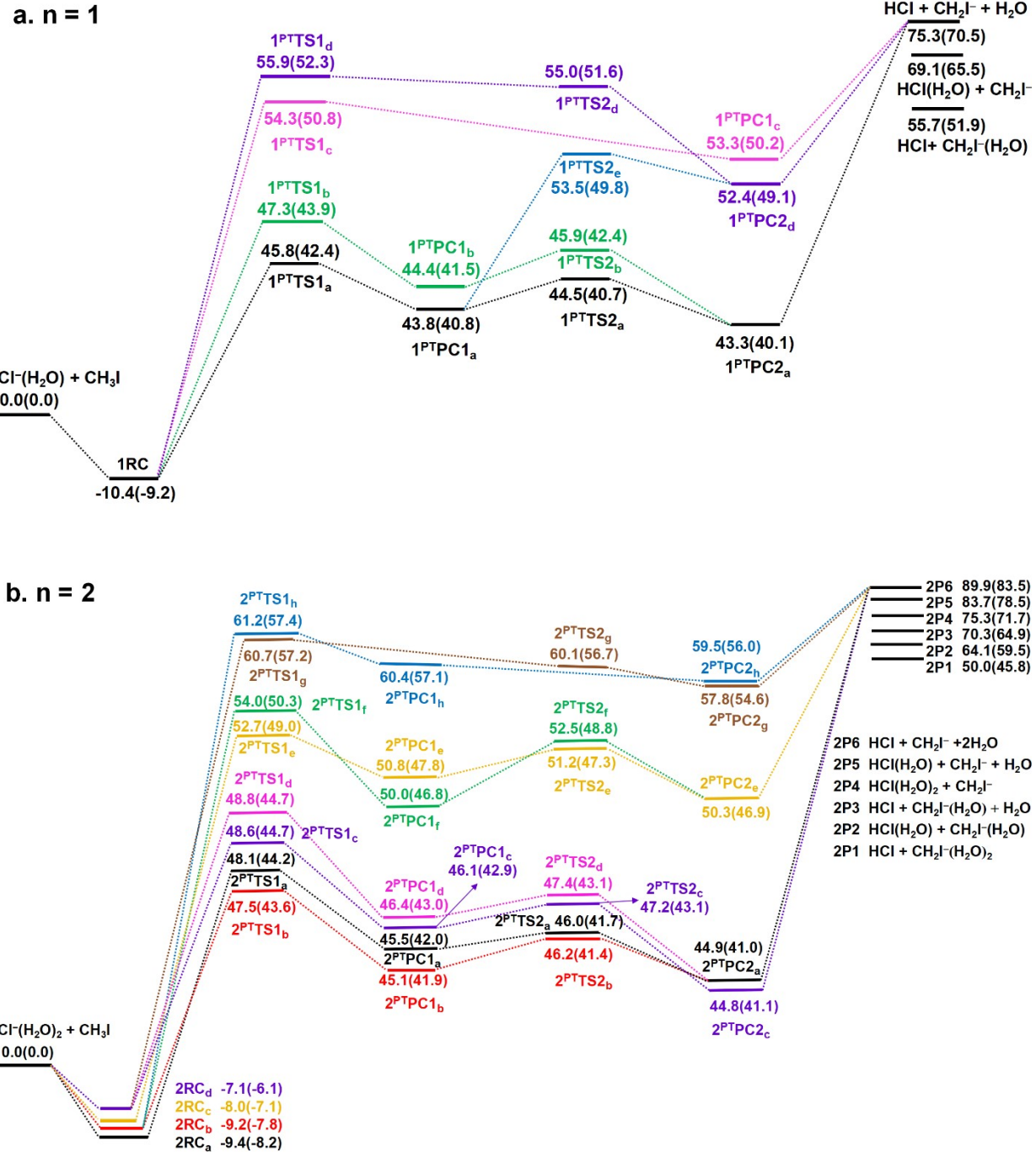
Figure S1. Potential energy profile of $Cl^-(H_2O)_{1,2}$ + CH_3I PT_{CH3} product channel at B97-1/ECP/d method. Calculated energy (in kcal/mol) values without zero-point energy (ZPE) are in normal text, and enthalpy values at 298.15 K are in parentheses.

a. n = 1

1RC 1^{PT}TS1$_a$ 1^{PT}TS1$_b$ 1^{PT}TS1$_c$ 1^{PT}TS1$_d$ 1^{PT}TS2$_a$

1TS2$_b$ 1TS2$_d$ 1TS2$_e$ 1PC1$_a$ 1PC1$_b$ 1PC1$_c$

1PC2$_a$ 1PC2$_d$

b. n = 2

2RC$_a$ 2RC$_b$ 2RC$_c$ 2RC$_d$ 2^{PT}TS1$_a$ 2^{PT}TS1$_b$

2^{PT}TS1$_c$ 2^{PT}TS1$_d$ 2^{PT}TS1$_e$ 2^{PT}TS1$_f$ 2^{PT}TS1$_g$ 2^{PT}TS1$_h$

2^{PT}TS2$_a$ 2^{PT}TS2$_b$ 2^{PT}TS2$_c$ 2^{PT}TS2$_d$ 2^{PT}TS2$_e$ 2^{PT}TS2$_f$

2^{PT}TS2$_g$ 2^{PT}PC1$_a$ 2^{PT}PC1$_b$ 2^{PT}PC1$_c$ 2^{PT}PC1$_d$ 2^{PT}PC1$_e$

2^{PT}PC1$_f$ 2^{PT}PC1$_h$ 2^{PT}PC2$_a$ 2^{PT}PC2$_c$ 2^{PT}PC2$_e$ 2^{PT}PC2$_g$ 2^{PT}PC2$_h$
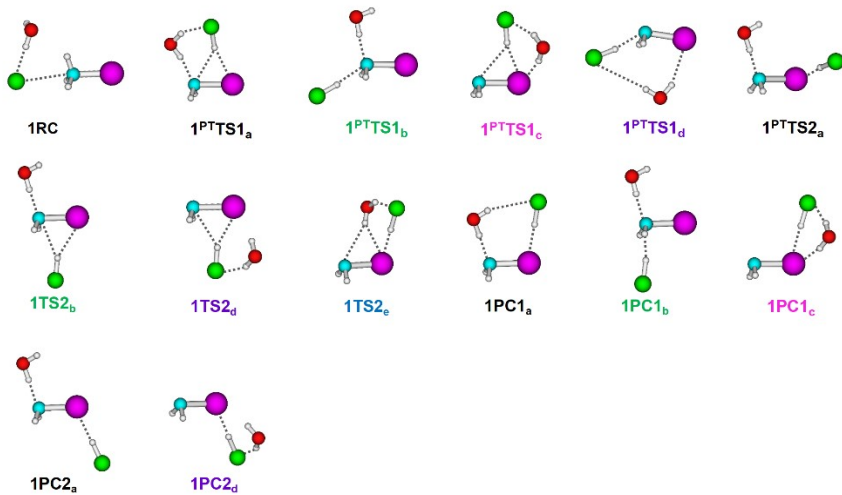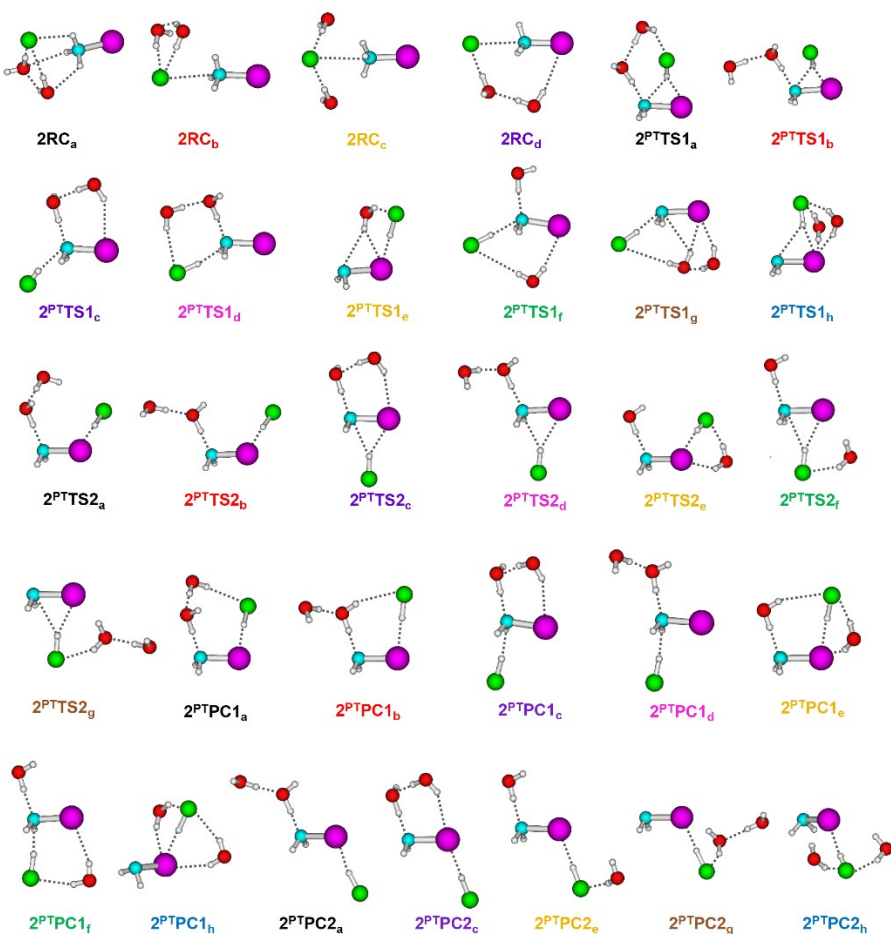
Figure S2. Structures of the stationary points for Cl$^-$(H$_2$O)$_{1,2}$ + CH$_3$I PT$_{CH3}$ product channel optimized at B97-1/ECP/d level of theory. Color code: H, white; C, blue; O, red; Cl, green; I, pink.
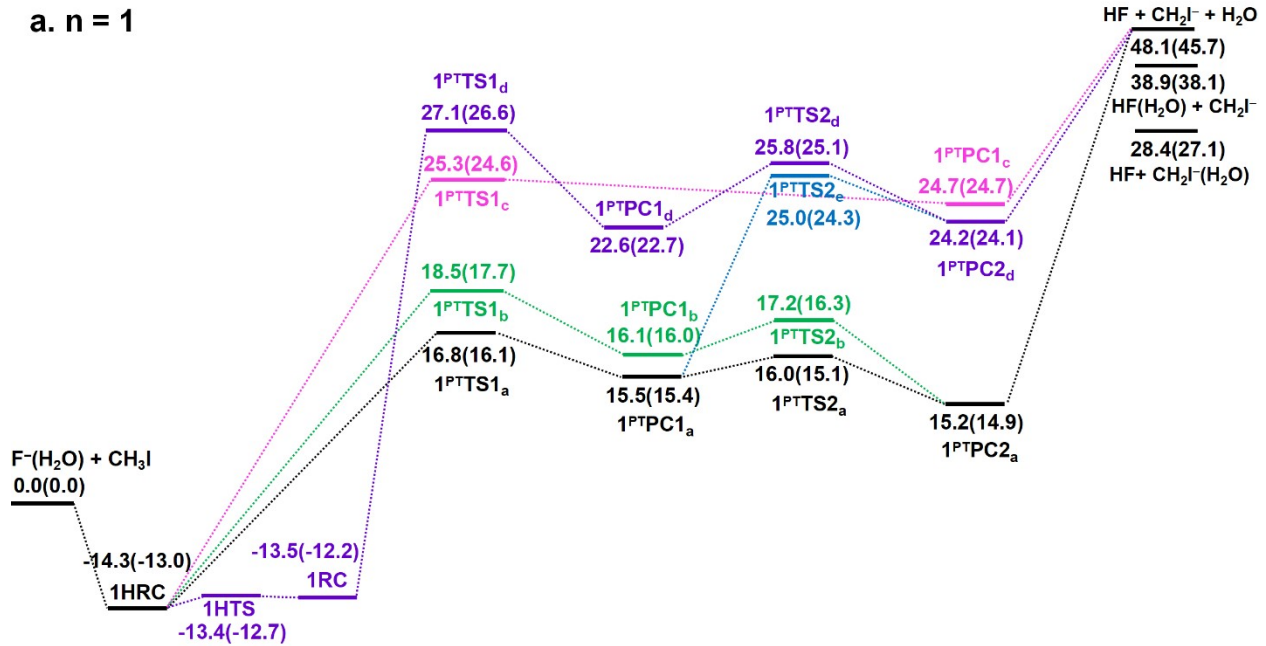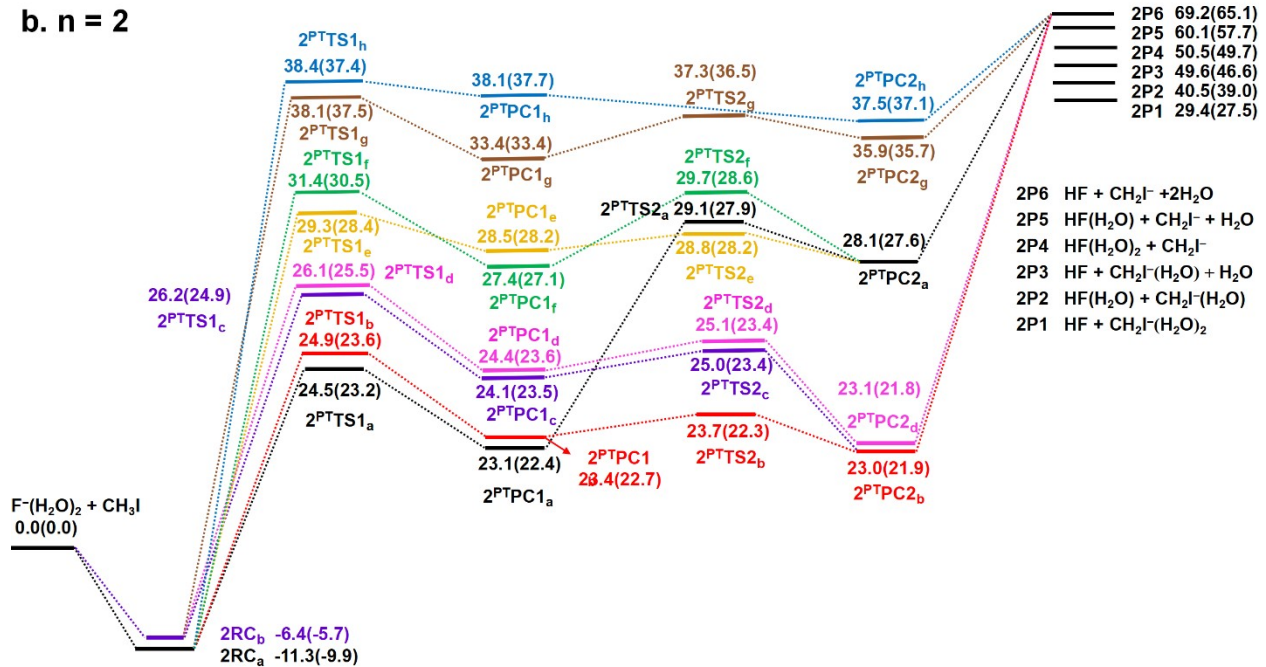
Figure S3. Potential energy profile of $F^-(H_2O)_{1,2} + CH_3I$ PT_{CH3} product channel at B97-1/ECP/d method. Calculated energy (in kcal/mol) values without zero-point energy (ZPE) are in normal text, and enthalpy values at 298.15 K are in parentheses.

a. n = 1

1HRC 1HTS 1RC $1^{PT}TS1_a$ $1^{PT}TS1_b$ $1^{PT}TS1_c$

$1^{PT}TS1_d$ $1^{PT}TS2_a$ $1^{PT}TS2_b$ $1^{PT}TS2_d$ $1^{PT}TS2_e$ $1^{PT}PC1_a$

$1^{PT}PC1_b$ $1^{PT}PC1_c$ $1^{PT}PC1_d$ $1^{PT}PC2_a$ $1^{PT}PC2_d$

b. n = 2

$2RC_a$ $2RC_b$ $2^{PT}TS1_a$ $2^{PT}TS1_b$ $2^{PT}TS1_c$ $2^{PT}TS1_d$

$2^{PT}TS1_e$ $2^{PT}TS1_f$ $2^{PT}TS1_g$ $2^{PT}TS1_h$ $2^{PT}TS2_a$ $2^{PT}TS2_b$

$2^{PT}TS2_c$ $2^{PT}TS2_d$ $2^{PT}TS2_e$ $2^{PT}TS2_f$ $2^{PT}TS2_g$ $2^{PT}PC1_a$

$2^{PT}PC1_b$ $2^{PT}PC1_c$ $2^{PT}PC1_d$ $2^{PT}PC1_e$ $2^{PT}PC1_f$ $2^{PT}PC1_g$

$2^{PT}PC1_h$ $2^{PT}PC2_a$ $2^{PT}PC2_b$ $2^{PT}PC2_d$ $2^{PT}PC2_g$ $2^{PT}PC2_h$
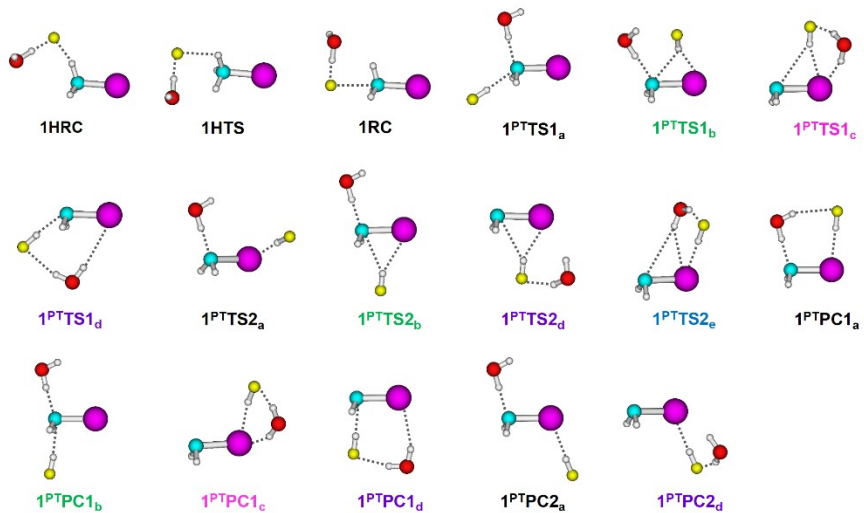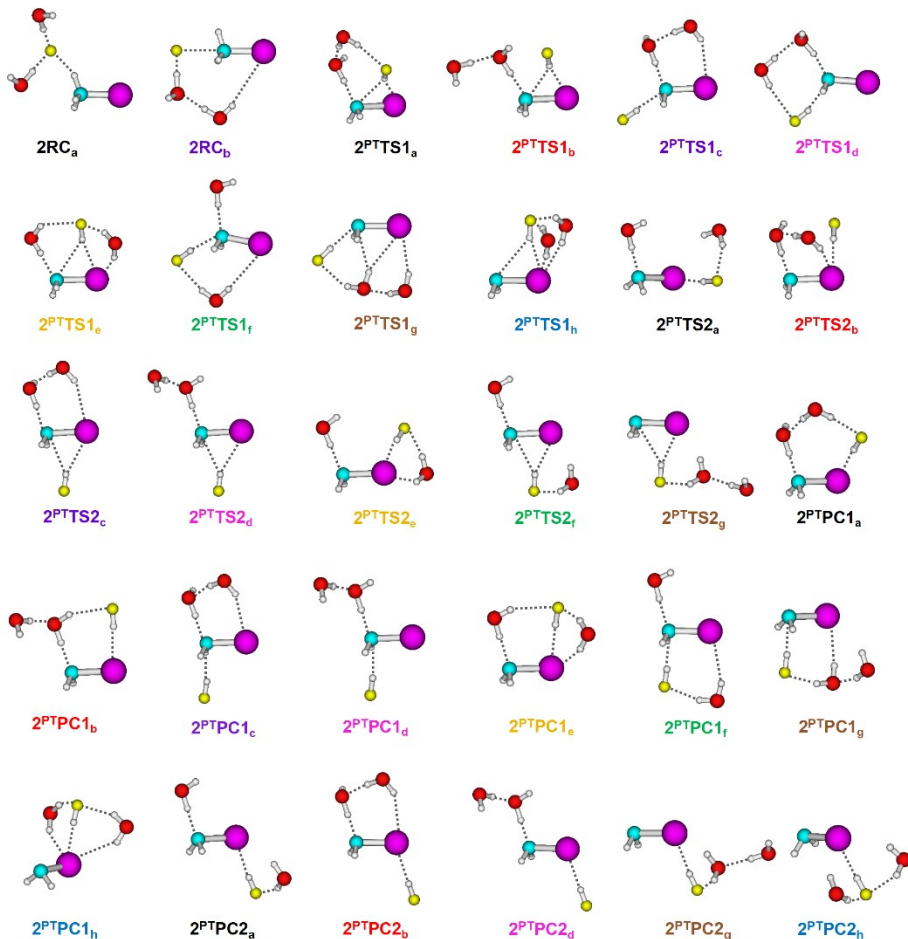
Figure S4. Structures of the stationary points for $F^-(H_2O)_{1,2} + CH_3I$ PT_{CH3} product channel optimized at B97-1/ECP/d level of theory. Color code: H, white; C, blue; O, red; F, yellow; I, pink.
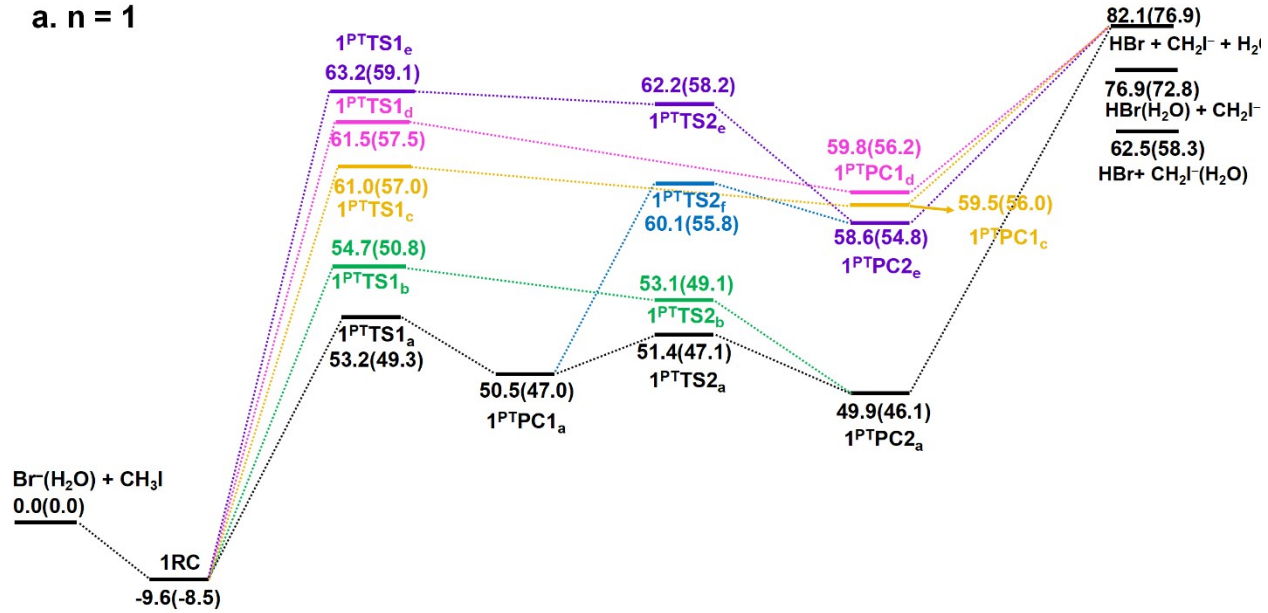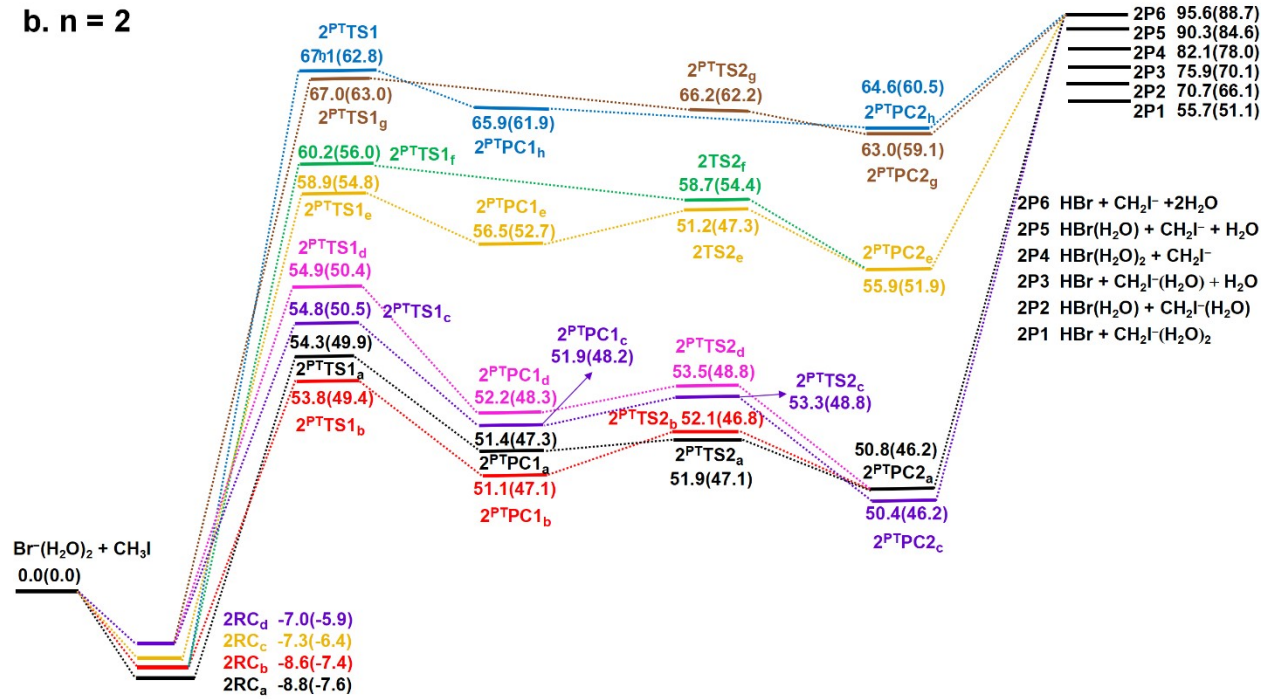
Figure S5. Potential energy profile of $Br^-(H_2O)_{1,2} + CH_3I$ PT_{CH3} product channel at B97-1/ECP/d method. Calculated energy (in kcal/mol) values without zero-point energy (ZPE) are in normal text, and enthalpy values at 298.15 K are in parentheses.

a. n = 1

1RC   1^{PT}TS1$_a$ 1^{PT}TS1$_b$ 1^{PT}TS1$_c$ 1^{PT}TS1$_d$ 1^{PT}TS1$_e$

1^{PT}TS2$_a$ 1^{PT}TS2$_b$ 1^{PT}TS2$_e$ 1^{PT}TS2$_f$ 1^{PT}PC1$_a$ 1^{PT}PC1$_c$

1^{PT}PC1$_d$ 1^{PT}PC2$_a$ 1^{PT}PC2$_e$

b. n = 2

2RC$_a$ 2RC$_b$ 2RC$_c$ 2RC$_d$ 2^{PT}TS1$_a$ 2^{PT}TS1$_b$

2^{PT}TS1$_c$ 2^{PT}TS1$_d$ 2^{PT}TS1$_e$ 2^{PT}TS1$_f$ 2^{PT}TS1$_g$ 2^{PT}TS1$_h$

2^{PT}TS2$_a$ 2^{PT}TS2$_b$ 2^{PT}TS2$_c$ 2^{PT}TS2$_d$ 2^{PT}TS2$_e$ 2^{PT}TS2$_f$

2^{PT}TS2$_g$ 2^{PT}PC1$_a$ 2^{PT}PC1$_b$ 2^{PT}PC1$_c$ 2^{PT}PC1$_d$ 2^{PT}PC1$_e$

2^{PT}PC1$_h$ 2^{PT}PC2$_a$ 2^{PT}PC2$_c$ 2^{PT}PC2$_e$ 2^{PT}PC2$_g$ 2^{PT}PC2$_h$
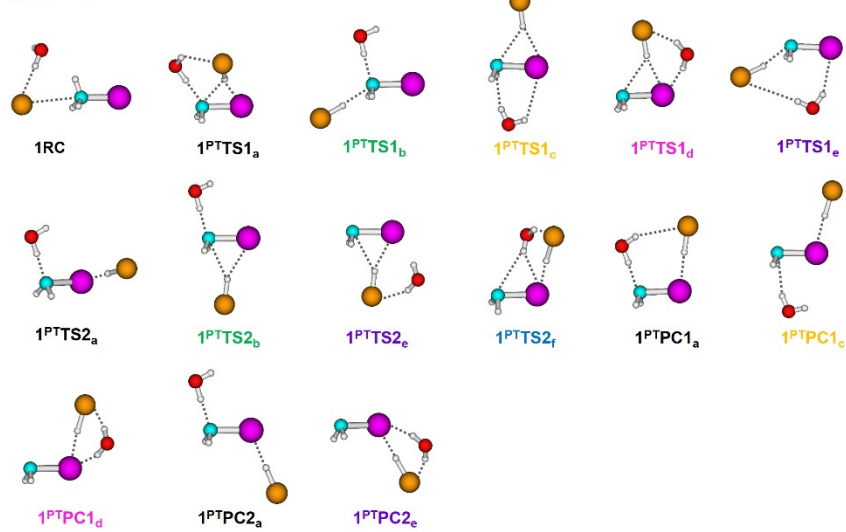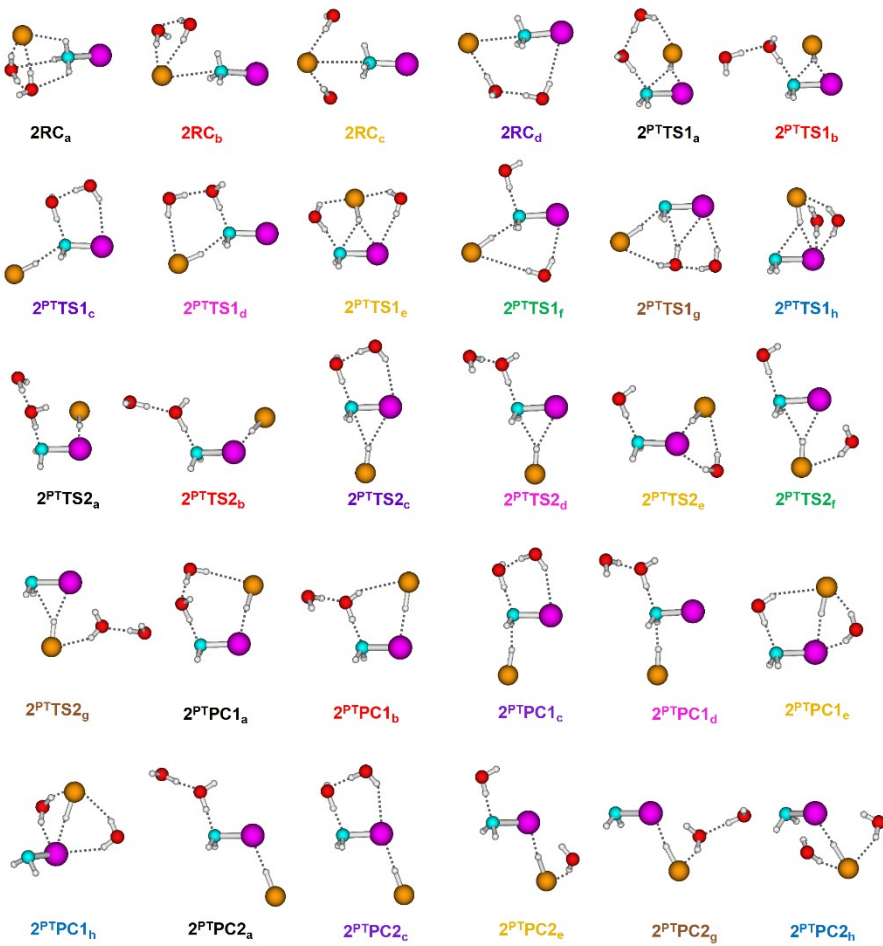
Figure S6. Structures of the stationary points for $Br^-(H_2O)_{1,2}$ + CH_3I PT$_{CH3}$ product channel optimized at B97-1/ECP/d level of theory. Color code: H, white; C, blue; O, red; Br, orange; I, pink.
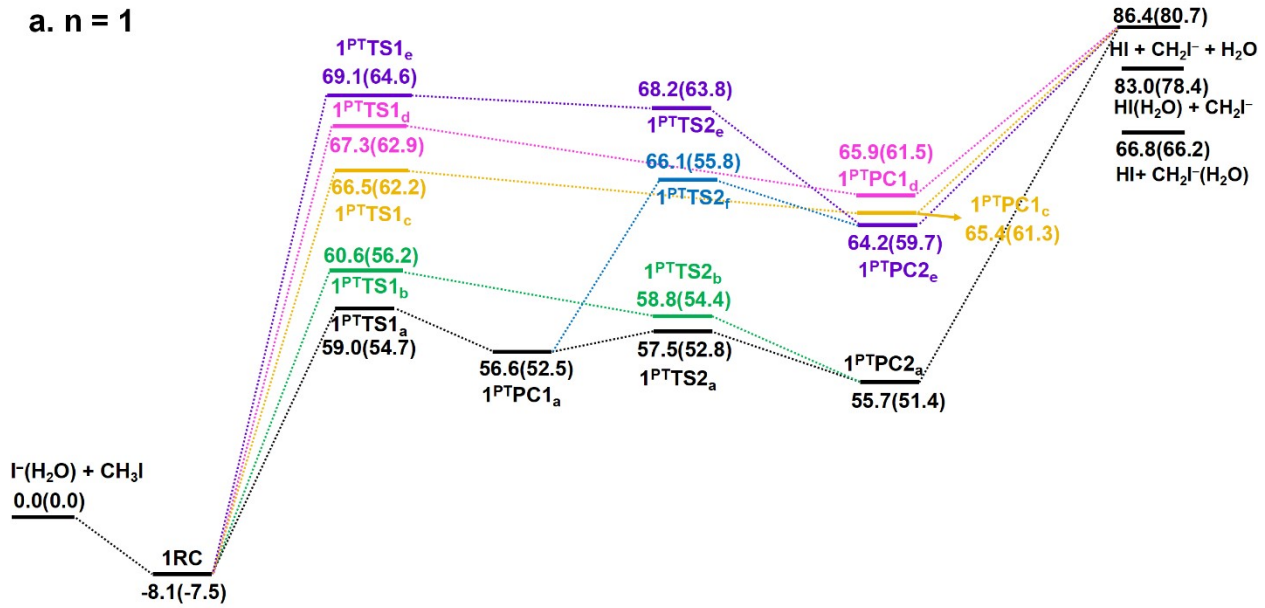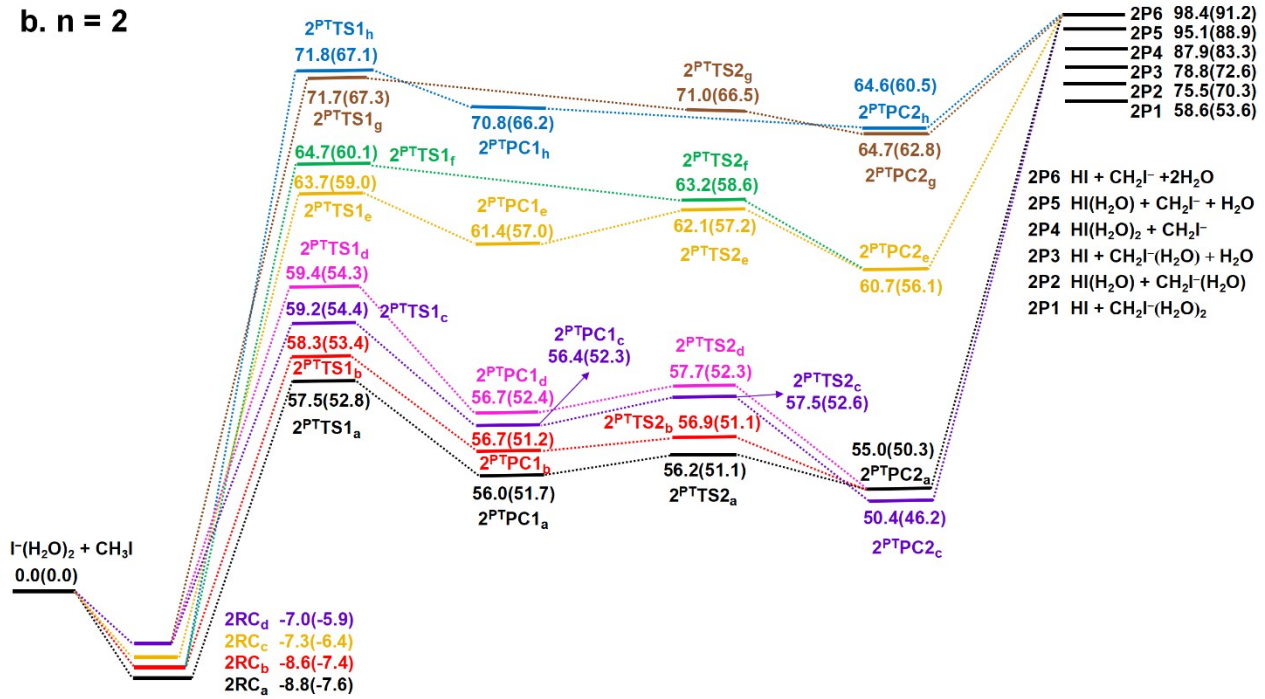
Figure S7. Potential energy profile of $I^-(H_2O)_{1,2} + CH_3I$ PT_{CH3} product channel at B97-1/ECP/d method. Calculated energy (in kcal/mol) values without zero-point energy (ZPE) are in normal text, and enthalpy values at 298.15 K are in parentheses.

a. n = 1

1RC   1^{PT}TS1$_a$ 1^{PT}TS1$_b$ 1^{PT}TS1$_c$ 1^{PT}TS1$_d$ 1^{PT}TS1$_e$

1^{PT}TS2$_a$ 1^{PT}TS2$_b$ 1^{PT}TS2$_e$ 1^{PT}TS2$_f$ 1^{PT}PC1$_a$ 1^{PT}PC1$_c$

1^{PT}PC1$_d$ 1^{PT}PC2$_a$ 1^{PT}PC2$_e$

b. n = 2

2RC$_a$ 2RC$_b$ 2RC$_c$ 2RC$_d$ 2^{PT}TS1$_a$ 2^{PT}TS1$_b$

2^{PT}TS1$_c$ 2^{PT}TS1$_d$ 2^{PT}TS1$_e$ 2^{PT}TS1$_f$ 2^{PT}TS1$_g$ 2^{PT}TS1$_h$

2^{PT}TS2$_a$ 2^{PT}TS2$_b$ 2^{PT}TS2$_c$ 2^{PT}TS2$_d$ 2^{PT}TS2$_e$ 2^{PT}TS2$_f$

2^{PT}TS2$_g$ 2^{PT}PC1$_a$ 2^{PT}PC1$_b$ 2^{PT}PC1$_c$ 2^{PT}PC1$_d$ 2^{PT}PC1$_e$

2^{PT}PC1$_h$ 2^{PT}PC2$_a$ 2^{PT}PC2$_c$ 2^{PT}PC2$_e$ 2^{PT}PC2$_g$ 2^{PT}PC2$_h$
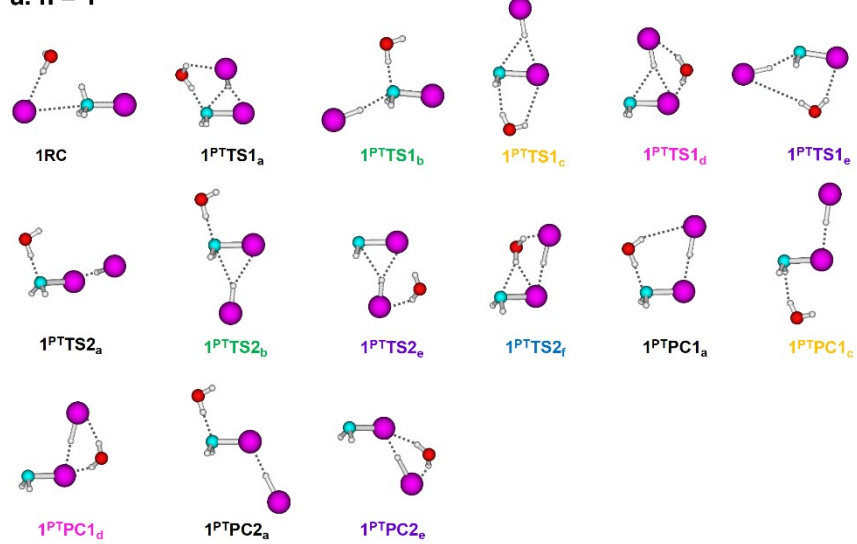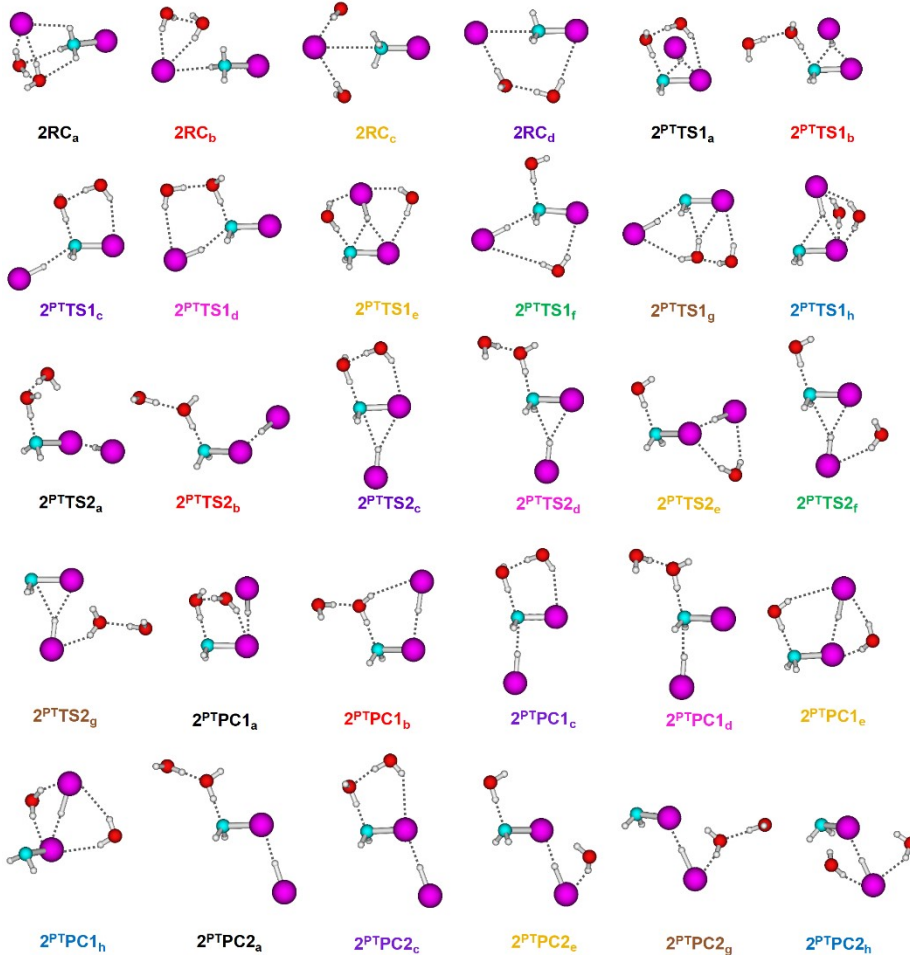
Figure S8. Structures of the stationary points for I$^-$(H$_2$O)$_{1,2}$ + CH$_3$I PT$_{CH3}$ product channel optimized at B97-1/ECP/d level of theory. Color code: H, white; C, blue; O, red; I, pink.
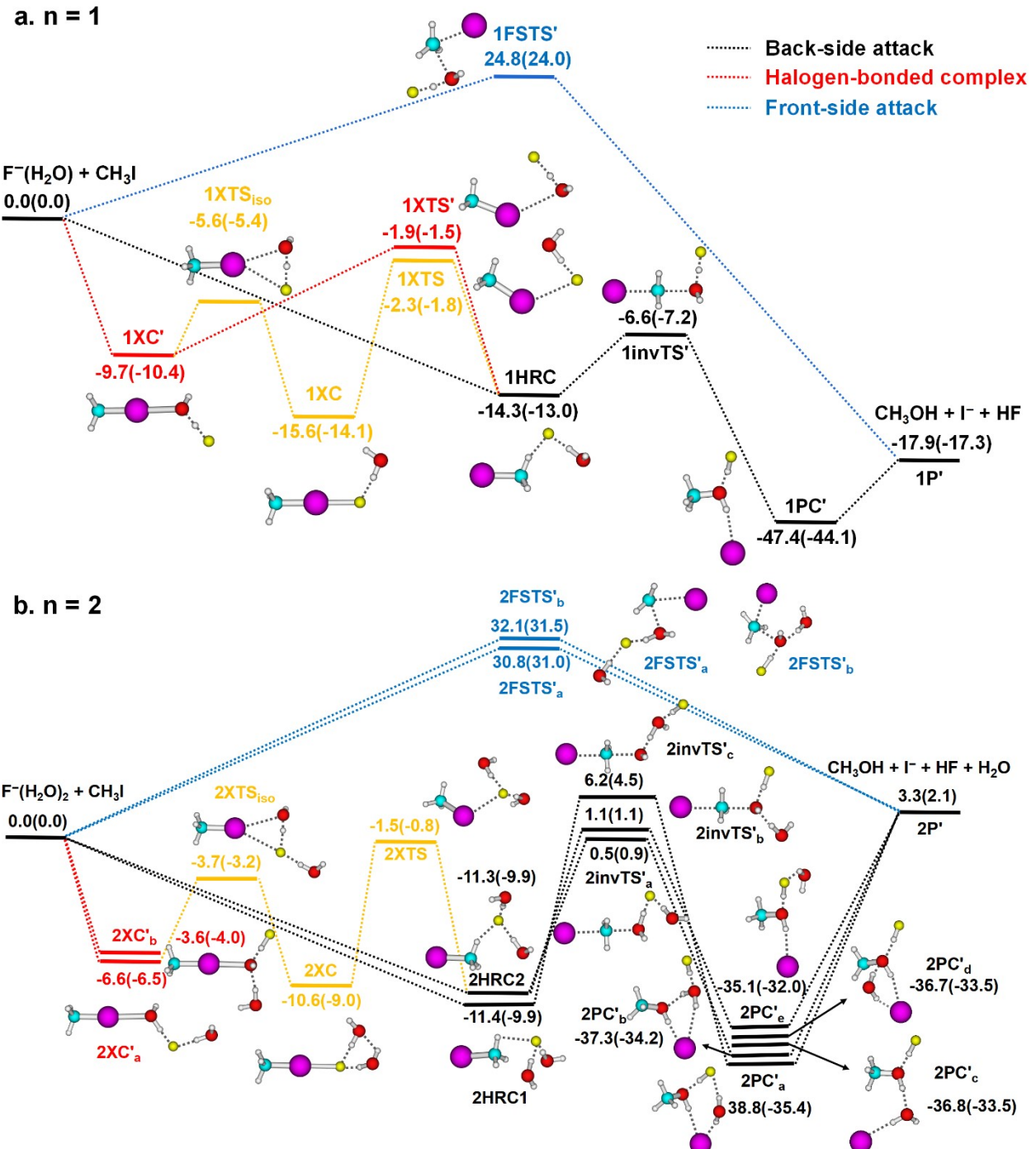
Figure S9. Potential energy profile of OH⁻-S$_N$2 product channel for the F⁻(H$_2$O)$_{1,2}$ + CH$_3$I reaction at B97-1/ECP/d level of theory. Values without ZPE are in normal text and enthalpy values at 298.15 K are in parentheses. Color code: H, white; C, blue; O, red; F, yellow; I, pink.
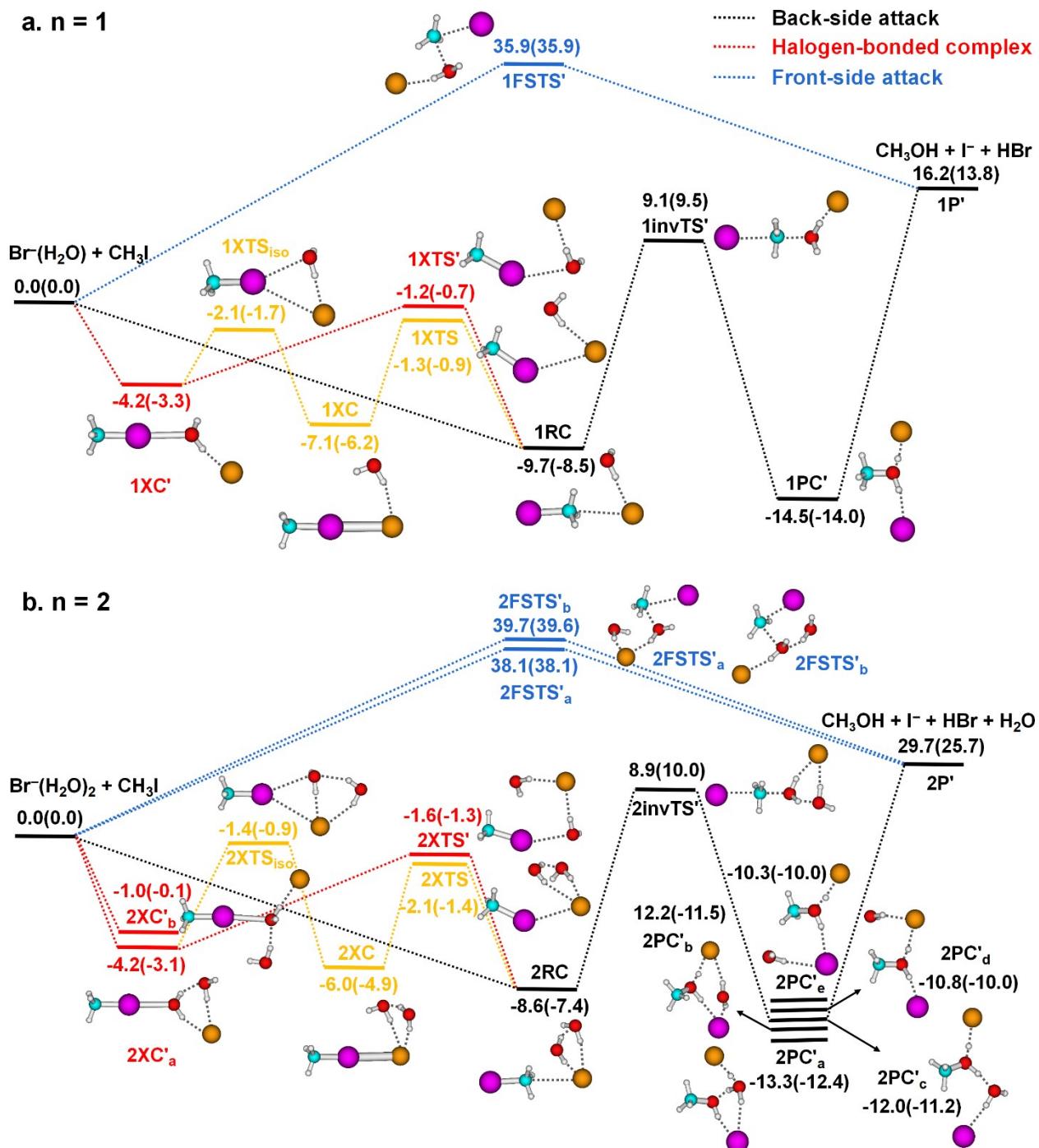
Figure S10. Potential energy profile of OH$^-$-S$_N$2 product channel for the Br$^-$(H$_2$O)$_{1,2}$ + CH$_3$I reaction at B97-1/ECP/d level of theory. Values without ZPE are in normal text and enthalpy values at 298.15 K are in parentheses. Color code: H, white; C, blue; O, red; Br, orange; I, pink.
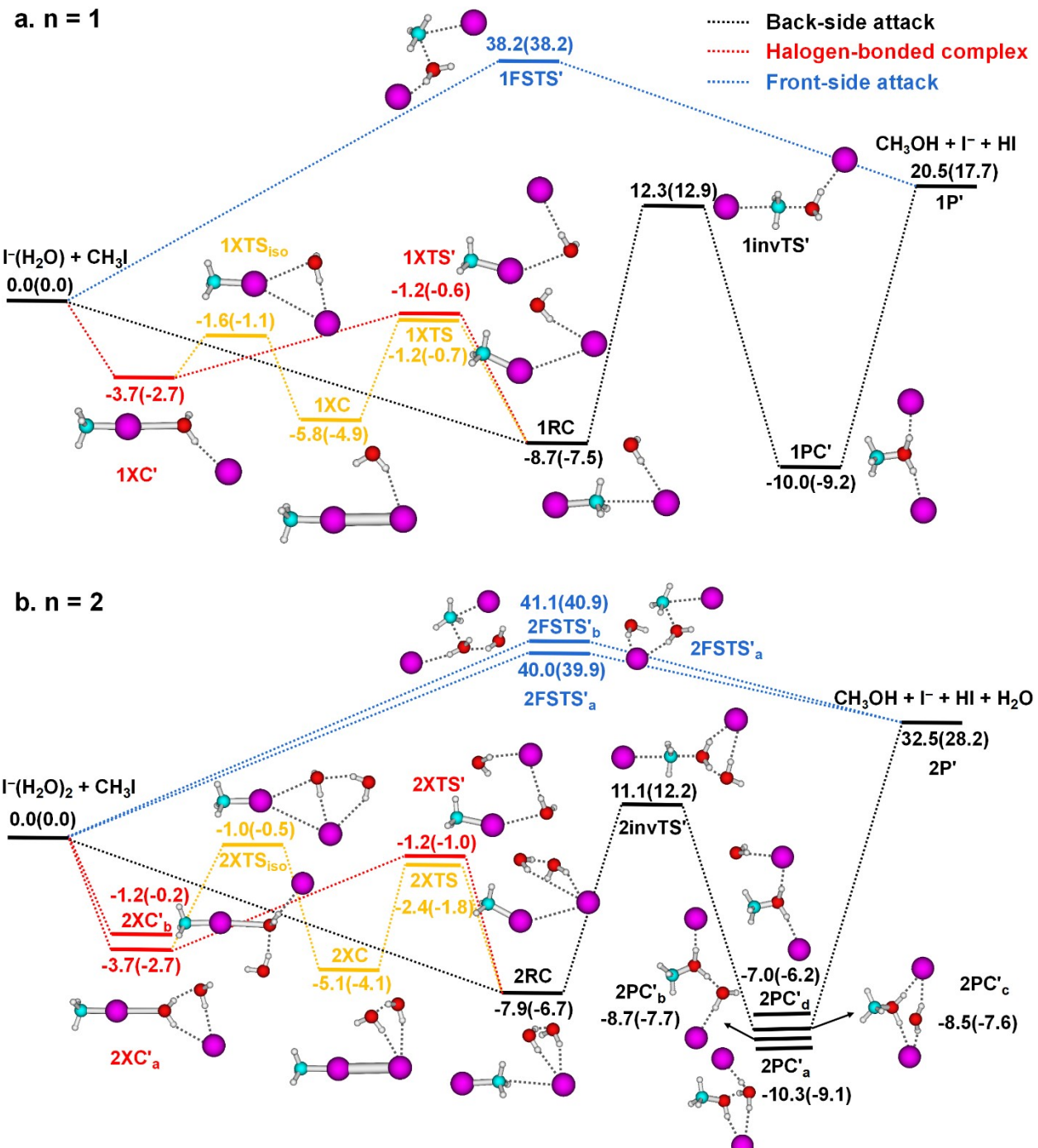
Figure S11. Potential energy profile of OH⁻-S$_N$2 product channel for the I⁻(H$_2$O)$_{1,2}$ + CH$_3$I reaction at B97-1/ECP/d level of theory. Values without ZPE are in normal text and enthalpy values at 298.15 K are in parentheses. Color code: H, white; C, blue; O, red; I, pink.

Figure S12. Plots of inv-S_N2 barrier heights vs a) %L‡ and b) %AS‡, and inv-S_N2' barrier heights vs c) %L$^{‡'}$ and d) %AS$^{‡'}$ (color code: green, Y = F, orange, Y = Cl, purple, Y = Br, blue, Y = I; symbol code: hollow, n = 0, half down, n = 1, solid, n = 2)
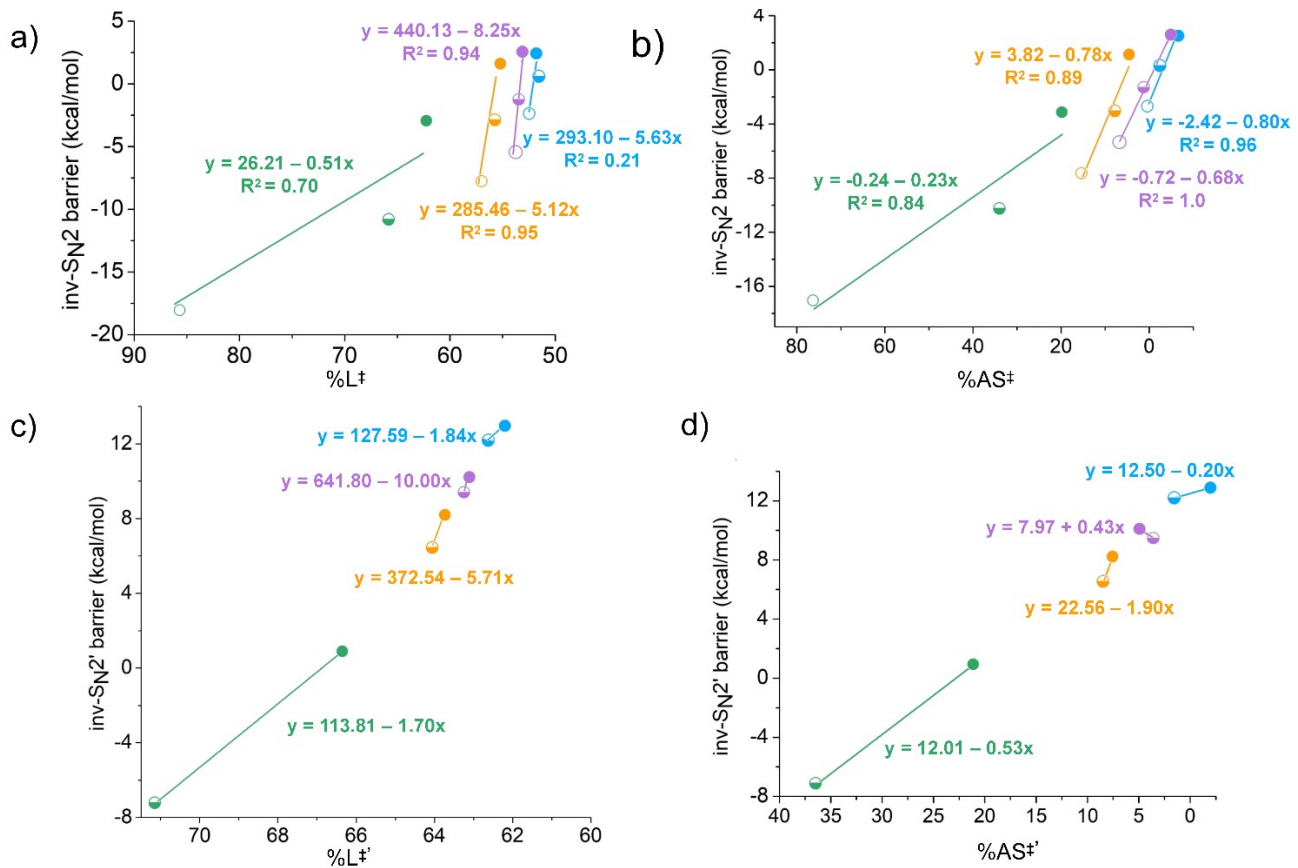
Figure S13. Donor and acceptor natural bond orbitals (NBOs) of the $[H_3C\text{---}I\text{---}OH_2(Y)]^-$ halogen-boned complex to illustrate the charge transfer interaction between I and O.

charge transfer

donor NBO
O, 2p orbital

acceptor NBO
C-I anti-bonding σ* orbital
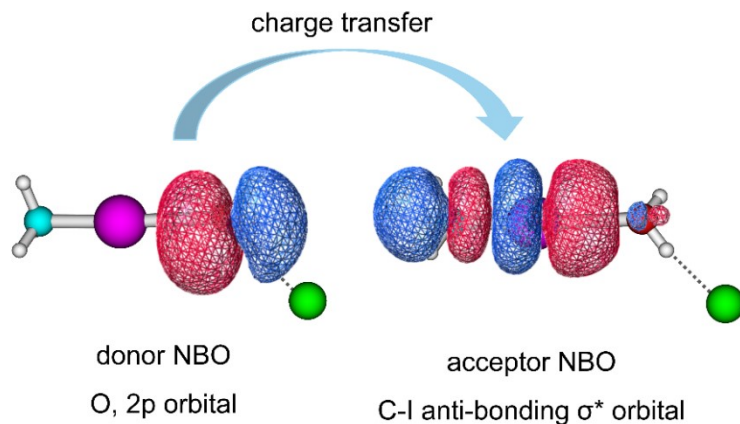
Table S11. The charge transfer stabilization energy between lone pair of nucleophile H_2O and C-I antibonding σ* orbital of the halogen-bond complexes $[H_3C\text{---}I\text{---}OH_2(Y)]^-$ as calculated under NBO scheme.

|	$E_{stablization}$ (kcal/mol)	
Y	n = 1	n = 2
F	14.98	10.43
Cl	7.69	7.33
Br	6.73	6.69
I	5.71	5.96
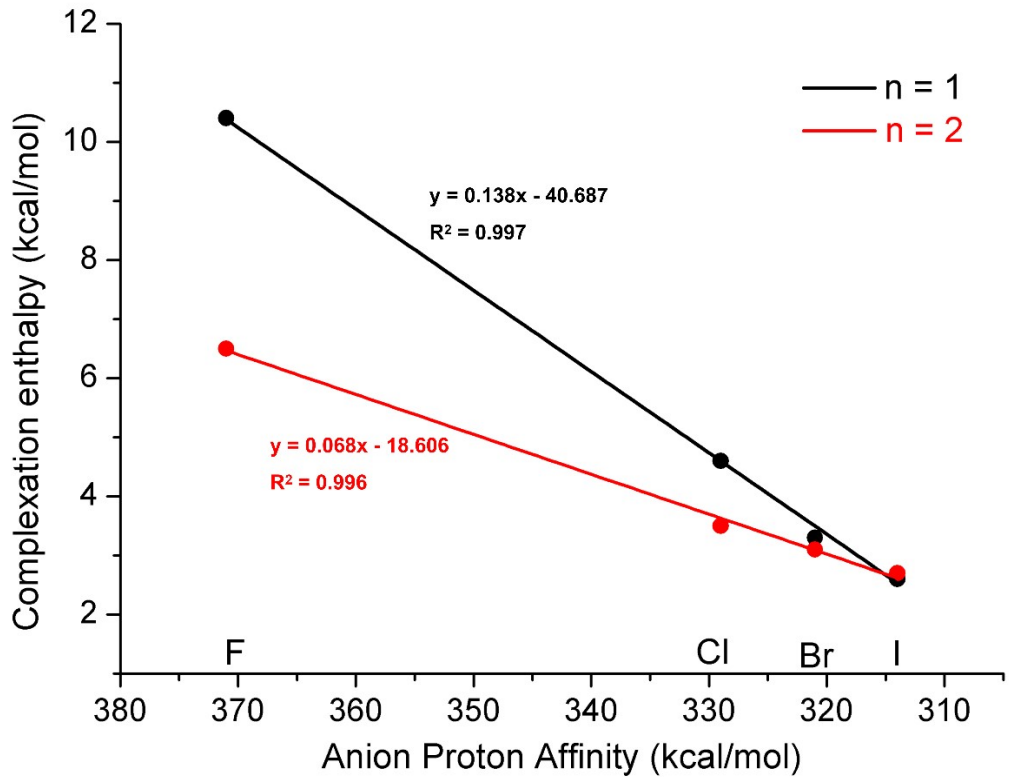
Figure S14. Complexation enthalpies of halogen-bonded complexes XC′ as a function of halogen anion proton affinity of the halogen-bonded complexes $[CH_3\text{---}I\text{---}OH_2(Y)]^-(H_2O)_{0,1}$.

a. back-side attack transition state (invTS′)
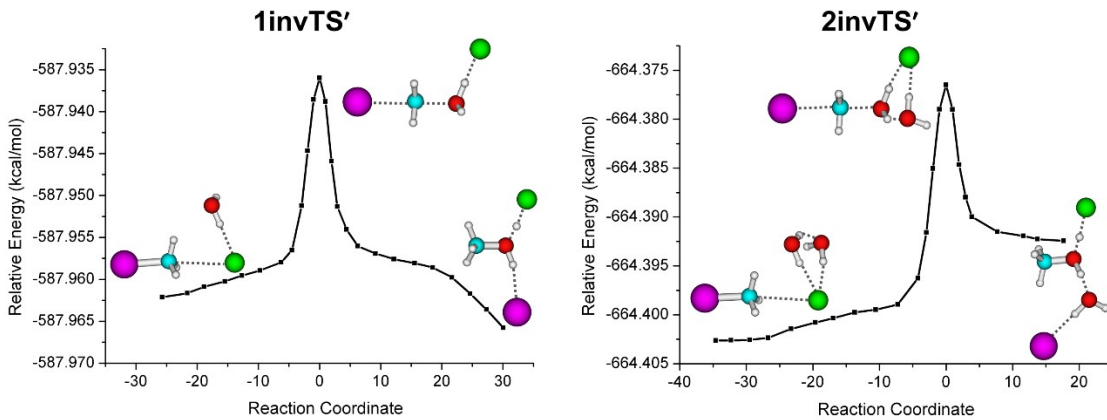

b. Halogen-bonded complex transition state (XTS')
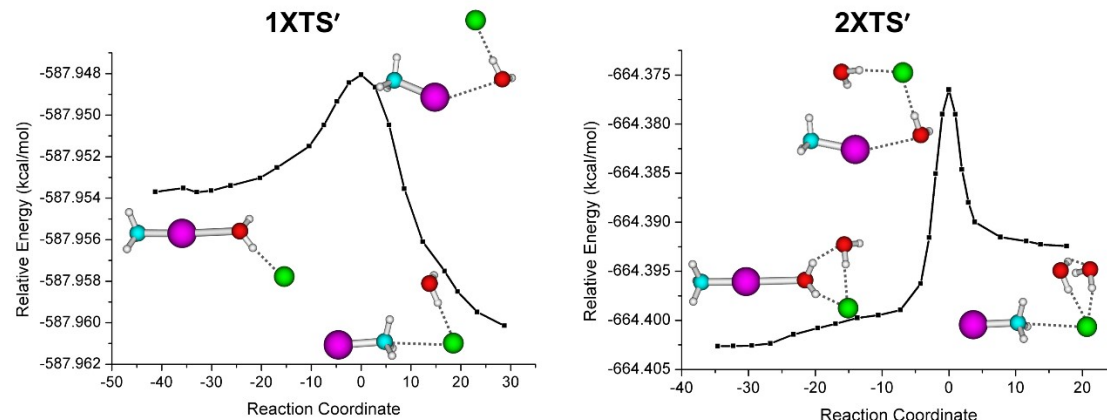
C. Halogen-bonded complexes inversion transition state (XTS$_{iso}$)
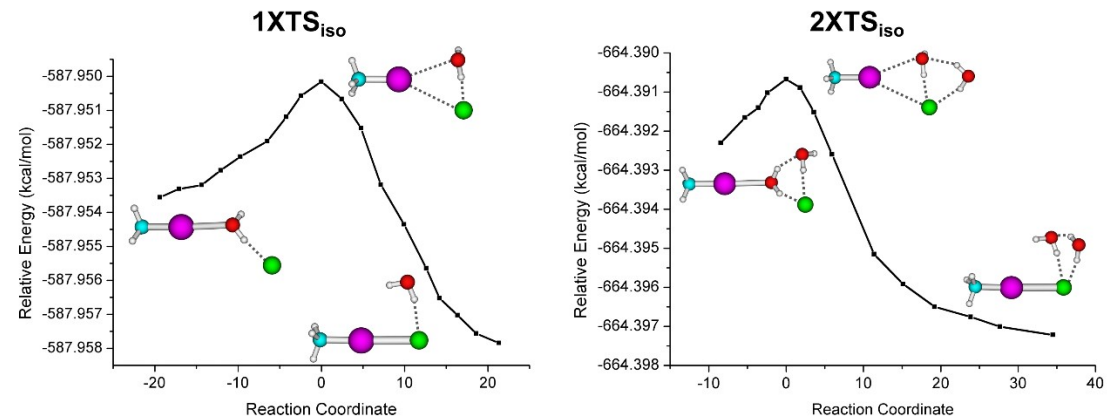
Figure S15. Intrinsic reaction coordinates (IRC) calculation of the invTS′, XTS′, and XTS$_{iso}$ Cl$^-$(H$_2$O)$_{n=1,2}$ + CH$_3$I S$_N$2 reaction using B97-1/ECP/d method.
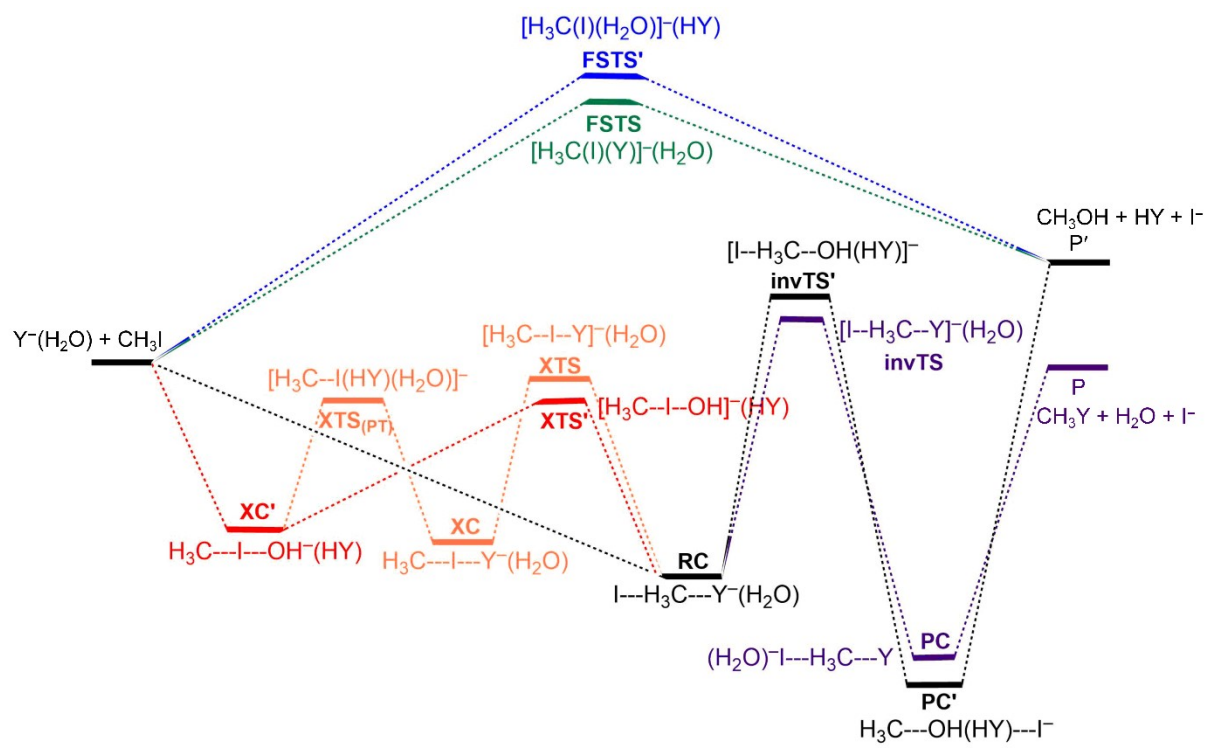
Scheme S1. Potential energy profile of Y^--S_N2 and HO^--S_N2 product channels for the $Y^-(H_2O)$ + CH_3I reaction proceeding with back-side attack (black), front-side attack at carbon (blue), and halogen-bonded complex (red) mechanisms.